Projected shell model description of high spin states in ^{124}Ce

Rani Devi, B. D. Sehgal, and S. K. Khosa
Department of Physics and Electronics, University of Jammu, Jammu 180006, India

J. A. Sheikh
Department of Physics, Kashmir University, Srinagar 190006, India

(Received 23 July 2005; published 13 December 2005)

The projected shell model is used to study the positive parity bands in ^{124}Ce. The energy spectra, transition quadrupole moments, and gyromagnetic factors are calculated. The calculation reproduces the observed positive parity bands. The peak in g-factors at spin $I = 14$ is predicted due to proton alignment arising from the two quasiparticle (2-qp) band crossing. The wave functions of yrast states at $I = 14$ to 20 are dominated by the two quasiparticle (2-qp) states. Measurement of transition quadrupole moments and g-factors would be a strong test for our predictions.

DOI: 10.1103/PhysRevC.72.064304 PACS number(s): 21.60.Cs, 21.10.Ky, 21.10.Re, 27.60.+j

I. INTRODUCTION

Recently, high-spin states have been studied in the very neutron-deficient ^{124}Ce isotope using the Gammasphere γ-ray spectrometer, together with the Microball charged-particle detector [1]. The level structure of ^{124}Ce has been extended to high spin ($30\hbar$) above the ground state and several new bands have been identified. The alignments of pairs of $h_{11/2}$ neutrons and protons are observed. For the interpretation of the new data, it is required for theoretical model to be able to well describe not only the yrast band but also side bands. Thus, the high spin data may be used as a crucial test for the existing models. In the past, very little theoretical effort has been put into the study of neutron-deficient ^{124}Ce as compared to other isotopes in mass $A = 120-130$ region. Recently, the rotational band structure and alignments of ^{124}Ce has been investigated by using cranked shell model (CSM) [1]. The CSM calculations predict neutron alignment in ^{124}Ce, which is not clear experimentally. In CSM calculations, the configuration assignment to higher spin states is not clear.

In recent years, the projected shell model (PSM) [2] has become quite successful in explaining a broad range of properties of deformed nuclei in various regions of nuclear Periodic Table. The most striking aspect of this quantum mechanical model is its ability to describe the finer details of high-spin spectroscopy data with simple physical interpretations. The advantage in this method is that the numerical requirement is minimal. The PSM approach is based on the diagonalization in the angular momentum projected basis from the deformed Nilsson states. The PSM has been systematically applied to study the rare-earth nuclei [3,4] and the agreement between the PSM results and experimental data has been found to be quite good.

The purpose of the present work is to interpret the positive parity bands observed in ^{124}Ce in the framework of PSM and also to test the applicability of this model in the $A = 120-130$ mass region. In the present study, the results are obtained for the energy spectrum, transition quadrupole moments, and gyromagnetic factors. It is for the first time that PSM has been applied to study ^{124}Ce nucleus. The work to study other nuclei in $A = 120-130$ mass region is in progress. The paper is organized as follows. In Sec. II, we shall give an outline of the PSM. This section also gives expressions for various physical quantities to be discussed in this paper. The results of calculations and comparisons with the experimental data are presented in Sec. III. Finally, the conclusions are given in Sec. IV.

II. PROJECTED SHELL MODEL

The detailed description of PSM can be found in a review article [2]. The PSM is based on the spherical shell model concept. It differs from the conventional shell model in that the PSM uses the angular momentum projected states as the basis for the diagonalization of the shell model Hamiltonian.

The wave function in the PSM is given by

$$|\sigma, IM\rangle = \sum_{K,\kappa} f_\kappa^\sigma \hat{P}^I_{\rm MK}|\phi_\kappa\rangle. \tag{1}$$

The index σ labels the states with same angular momentum and κ the basis states. $P^I_{\rm MK}$ is angular momentum projection operator and f_κ^σ are the weights of the basis states κ. We have assumed axial symmetry for the basis states and the intrinsic states are, therefore, the eigenstates of the K-quantum number. For calculations of an even-even system, the following four kinds of basis states $|\phi_\kappa\rangle$ are considered: the quasiparticle (qp) vacuum $|0\rangle$, two-quasineutron states $a^\dagger_{\nu1}a^\dagger_{\nu2}|0\rangle$, two-quasiproton states $a^\dagger_{\pi1}a^\dagger_{\pi2}|0\rangle$, and two-quasineutron plus two-quasiproton (or 4-qp) states $a^\dagger_{\nu1}a^\dagger_{\nu2}a^\dagger_{\pi1}a^\dagger_{\pi2}|0\rangle$. The projected vacuum $|0\rangle$, for instance, is the ground-state band (g-band) of an even-even nucleus.

The weight factors, f_κ^σ in Eq. (1), are determined by diagonalization of the shell model Hamiltonian in the space spanned by the projected basis states given above. This leads to the eigenvalue equation

$$\sum_{\kappa'}(H_{\kappa\kappa'} - E_\sigma N_{\kappa\kappa'})f^\sigma_{\kappa'} = 0, \tag{2}$$

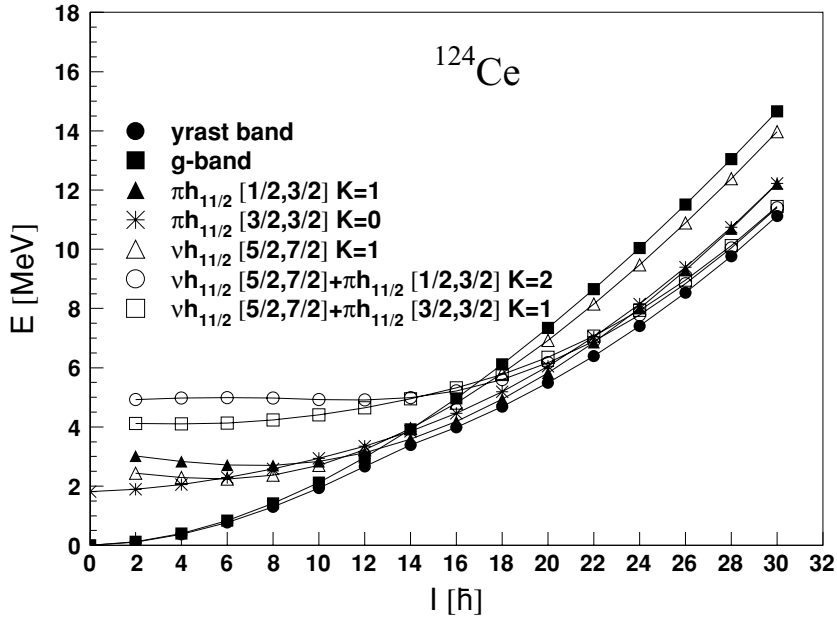

FIG. 1. Band diagram for selected positive parity configurations.

and the normalization is chosen such that

$$\sum_{\kappa\kappa'} f^{\sigma}_{\kappa} N_{\kappa\kappa'} f^{\sigma'}_{\kappa'} = \delta_{\sigma\sigma'}, \tag{3}$$

where the Hamiltonian and norm-matrix elements are given by

$$H_{\kappa\kappa'} = \langle\phi_\kappa|\hat{H}\hat{P}^{I}_{K_\kappa K_{\kappa'}}|\phi_{\kappa'}\rangle, \tag{4}$$

$$N_{\kappa\kappa'} = \langle\phi_\kappa|\hat{P}^{I}_{K_\kappa K_{\kappa'}}|\phi_{\kappa'}\rangle. \tag{5}$$

In the numerical calculations, we have used the standard quadrupole-quadrupole plus (monopole and quadrupole) pairing force, i.e.,

$$\hat{H} = \hat{H}_0 - \frac{1}{2}\chi\sum_{\mu}\hat{Q}^{\dagger}_{\mu}\hat{Q}_{\mu} - G_M\hat{P}^{\dagger}P - G_Q\sum_{\mu}\hat{P}^{\dagger}_{\mu}\hat{P}_{\mu}, \tag{6}$$

where $\hat{H}_0$ is the spherical single-particle Hamiltonian. The strength of the quadrupole force χ is adjusted such that the known quadrupole deformation parameter ϵ_2 is obtained. This condition results from the mean-field approximation of the quadrupole-quadrupole interaction of the Hamiltonian in Eq. (6). The monopole pairing force constants G_M are adjusted to give the known energy gaps. For all the calculations, we have used [6]

$$G^{\nu}_{M} = \left[19.60 - 15.70\frac{N-Z}{A}\right]A^{-1}, \quad G^{\pi}_{M} = 19.60A^{-1}. \tag{7}$$

The strength parameter G_Q for quadrupole pairing is assumed to be proportional to G_M. In the present calculations, it is taken as 0.20.

Electromagnetic transitions can give important information on the nuclear structure and provide a stringent test of a particular model. In the present work, we have calculated the electromagnetic properties using PSM approach. The reduced transition probabilities $B(EL)$ from the initial state (σ_i, I_i) to the final state (σ_f, I_f) are given by [4]

$$B(EL, I_i \longrightarrow I_f) = \frac{e^2}{(2I_i+1)}|\langle\sigma_f, I_f\|\hat{Q}_L\|\sigma_i, I_i\rangle|^2, \tag{8}$$

where the reduced matrix element is given by [4]

$$\begin{aligned}\langle\sigma_f, I_f\|\hat{Q}_L\|\sigma_i, I_i\rangle &= \sum_{\kappa_i,\kappa_f} f^{\sigma_i}_{\kappa_i} f^{\sigma_f}_{\kappa_f} \sum_{M_i,M_f,M} (-)^{I_f - M_f} \\ &\times \begin{pmatrix} I_f & L & I_i \\ -M_f & M & M_i \end{pmatrix} \\ &\times \left\langle\phi_{\kappa_f}\middle|\hat{P}^{I_f}_{K_{\kappa_f}M_f}\hat{Q}_{LM}\hat{P}^{I_i}_{K_{\kappa_i}M_i}\middle|\phi_{\kappa_i}\right\rangle \\ &= 2\sum_{\kappa_i,\kappa_f} f^{\sigma_i}_{\kappa_i} f^{\sigma_f}_{\kappa_f} \sum_{M',M''} (-)^{I_f - K_{\kappa_f}}(2I_f+1)^{-1} \\ &\times \begin{pmatrix} I_f & L & I_i \\ -K_{\kappa_f} & M' & M'' \end{pmatrix} \int d\Omega D_{M''K_{\kappa_i}}(\Omega) \\ &\times \left\langle\phi_{\kappa_f}\middle|\hat{Q}_{LM'}\hat{R}(\Omega)\middle|\phi_{\kappa_i}\right\rangle. \end{aligned} \tag{9}$$

The transition quadrupole moment $Q_t(I)$ is related to the $B(E2)$ transition probability through

$$Q_t(I) = \left(\frac{16\pi}{5}\frac{B(E2, I \to I-2)}{\langle IK20|I-2K\rangle}\right)^{1/2}. \tag{10}$$

In the calculations, we have used the effective charges of $1.5e$ for protons and $0.5e$ for the neutrons.

Variation of Q_t with I can provide information on shape evolution in nuclei. In the case of a rigid rotor, the Q_t curve as a function of I is a straight line. Experimentally, one finds a deviation from the rigid body behavior for most of the neutron deficient Ce nuclei. One expects more or less a constant value in Q_t up to the first band crossing. At the band crossing, one often sees a dip in Q_t value due to a small overlap between the wave functions of the initial and the final states involved. There can be a change in Q_t values after the first band crossing, which indicates a shape induced by quasiparticle alignment.

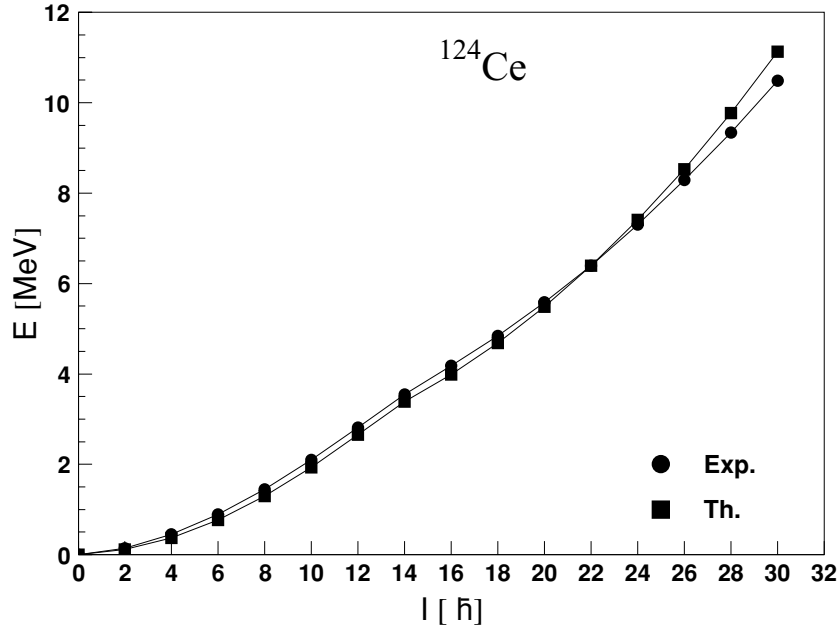

FIG. 2. Comparison of the calculated energies $E(I)$ of the yrast band with experimental data of ^{124}Ce. The calculated yrast band consists of the lowest states after diagonalization at each angular momentum I.

The other important electromagnetic quantity, which can give crucial information about the level occupancy and thus is a direct indication of the nature of alignment, is the gyromagnetic factor (g-factor). The g-factors $g(\sigma, I)$, $g_\pi(\sigma, I)$, and $g_\nu(\sigma, I)$ are defined by [4]

$$g(\sigma, I) = \frac{\mu(\sigma, I)}{\mu_N I} = g_\pi(\sigma, I) + g_\nu(\sigma, I) \tag{11}$$

with $g_\tau(\sigma, I)$, $\tau = \pi, \nu$ given by

$$g_\tau(\sigma, I) = \frac{1}{\mu_N [I(I+1)]^{1/2}} [g_l^\tau \langle \sigma, I \| \hat{J}^\tau \| \sigma, I \rangle + \left(g_s^\tau - g_l^\tau\right) \langle \sigma, I \| \hat{S}^\tau \| \sigma, I \rangle] \tag{12}$$

and $\mu(\sigma, I)$ is the magnetic moment of a state (σ, I). In our calculations, the following standard values of g_l and g_s have been taken: $g_l^\pi = 1$, $g_l^\nu = 0$, $g_s^\pi = 5.586 \times 0.75$, and $g_s^\nu = -3.826 \times 0.75$.

III. RESULTS AND DISCUSSION

The PSM calculations proceed in two steps. In the first step, an optimum set of deformed basis is constructed from the standard Nilsson potential. The Nilsson parameters are taken from Ref. [5] and the calculations are performed by considering three major shells ($N = 3, 4$, and 5) for both protons and neutrons. The basis deformation ϵ_2 is taken from the theoretical value of the total Routhian surface (TRS) calculations [1] as $\epsilon_2 = 0.292$ and $\epsilon_4 = 0.010$. The intrinsic states within the chosen energy window around the Fermi surface gives rise to the size of the basis space $|\phi_\kappa\rangle$, in Eq. (1) of the order of 67. In the second step, these basis states are

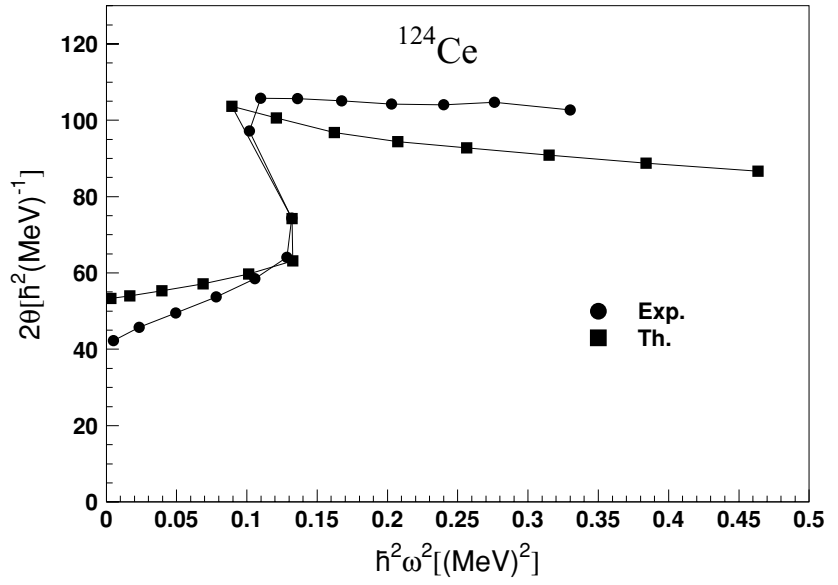

FIG. 3. Comparison of calculated moment of inertia 2θ with experimental data as a function of square of rotational frequency ω^2. These quantities are defined as $2\theta = \frac{2I-1}{\omega}$, $\omega = [E(I) - E(I-2)]/2$.

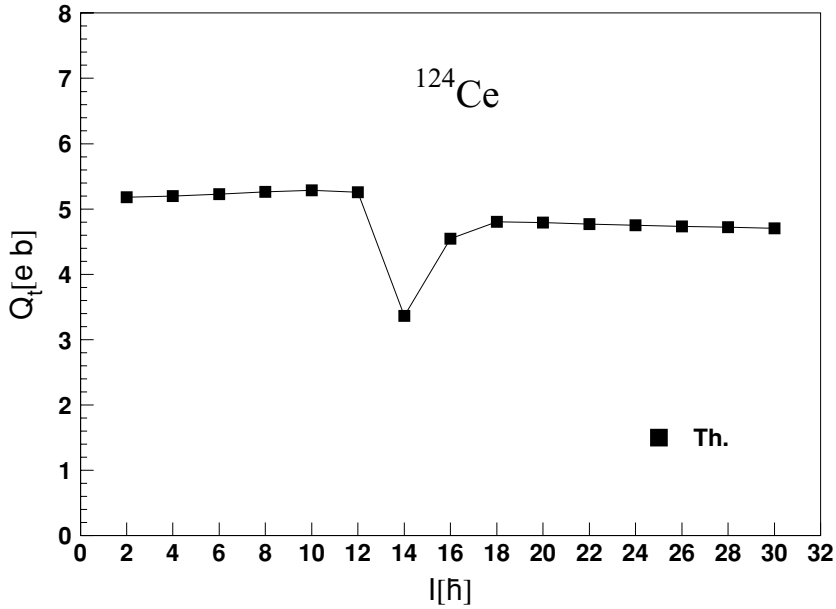

FIG. 4. The calculated transition quadrupole moments Q_t as a function of the angular momentum for the yrast band in ^{124}Ce.

projected to good angular-momentum states, and the projected basis is then used to diagonalize the shell model Hamiltonian. The band diagram [3] which gives the projected energies for the configurations close to the Fermi surface is shown in Fig. 1. For each band we have marked its quasiparticle configuration. (Since there are so many bands, only the most important ones are shown.) The proton 2-qp state $\pi h_{11/2}[1/2, 3/2]$ crosses the g-band around $I = 14$. This corresponds to the alignment of proton pairs as observed in the experiment. Again, around spin $I = 20$, two 4-qp bands becomes lowest and are nearly degenerate.

A. The yrast band

The yrast band consisting of the lowest energies after diagonalization at each spin, is plotted in Fig. 2 to compare with the experimental data. These values are also displayed in Fig. 3 in a sensitive plot of moment of inertia as a function of square of the rotational frequency. It can be seen from Figs. 2 and 3 that there is a very good agreement between the theory and experiment in both the plots. On the basis of PSM results, it is possible to assign configurations to yrast band as follows: For $I = 0-12\hbar$, yrast band is built upon the quasiparticle vacuum (0-qp) configuration; for $I = 14-22\hbar$, it corresponds to proton 2-qp $\pi h_{11/2}[1/2, 3/2]$ configuration; and for $I = 24$ to the experimentally observed limt ($30\hbar$), it corresponds to the 4-qp $\nu h_{11/2}[5/2, 7/2] + \pi h_{11/2}[1/2, 3/2]$ configuration.

In Figs. 4 and 5, the Q_t values and $B(E2)$ values are plotted as a function of spin I. The sudden fall in the Q_t at $I = 14$ may be thought to be associated with the first band crossing. Due to the occupation of the fully aligned orbitals after this band crossing, the Q_t values becomes smaller for the higher spin states. Similar trend is seen in the $B(E2)$ values. Above

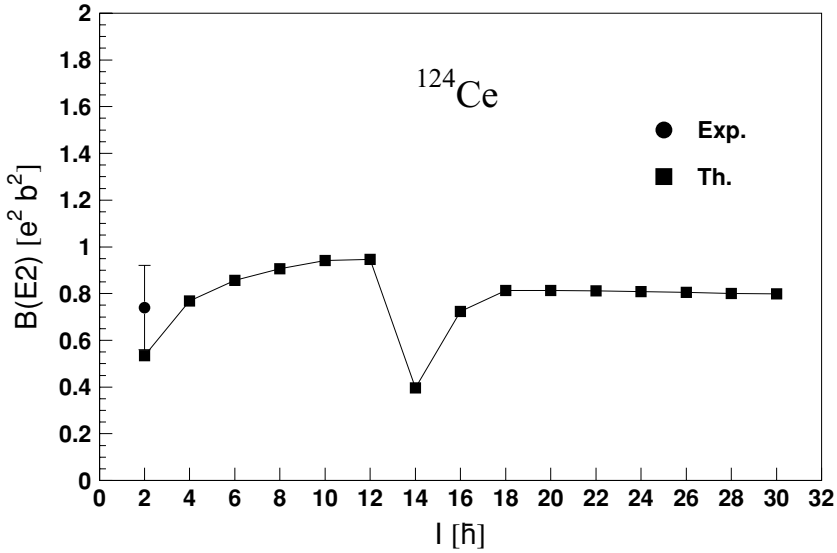

FIG. 5. The calculated $B(E2)$ values as a function of angular momentum for the yrast band in ^{124}Ce. The known experimental value of $2^+ \rightarrow 0^+$ transition 0.74(18) [7] $e^2\,b^2$ is in good agreement with the calculated value.

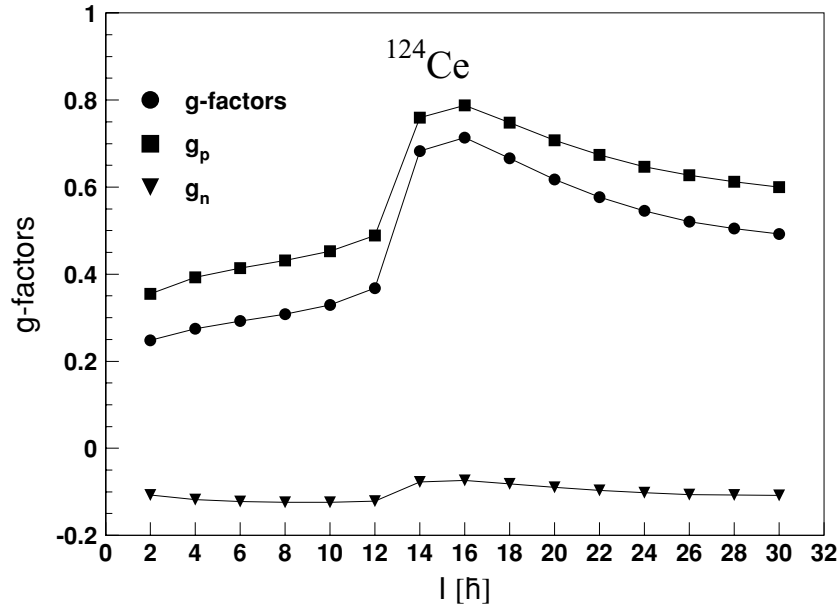

FIG. 6. The calculated g-factors as a function of angular momentum for the yrast band in ^{124}Ce.

$I = 20$, maximum contribution to yrast states comes from the configuration based on the 4-qp states.

In Fig. 6, the theoretical results on g-factors are displayed. As can be seen from Fig. 6, there is a pronounced peak in the g_n and g_p at spin 14 with a decreasing trend thereafter. This pronounced peak in g-factors is obviously due to the proton 2-qp band crossing at $I = 14$. Besides this, the positive value of total g-factor also indicates a proton alignment. Unfortunately, there is no experimental data to compare with.

B. Positive parity bands

In Fig. 7, the results of theoretical calculation of energies of positive parity bands are presented along side the experimentally observed bands. The theoretical results have been obtained by the diagonalization of the Hamiltonian Eq. (6) in the projected basis. The experimental bands have been taken from Ref. [1]. It is important to point out here that present PSM calculation involves mixing amongst as many as 67 bands as a result of which nonaxiality creeps into the present results. Further, PSM technique involves exact angular momentum projection. On comparison, it is observed that the present calculation agrees well with the experimental spectra. An analysis and critical examination of the wave functions reveals that all the states belonging to a particular band do not belong to a single configuration. They arise from a superposition of different configurations with different weight factors. It was pointed out by Smith *et al*. [1] who performed cranked Woods-Saxon (CWS) calculations that each of these bands could be assigned a single configuration. They assigned different

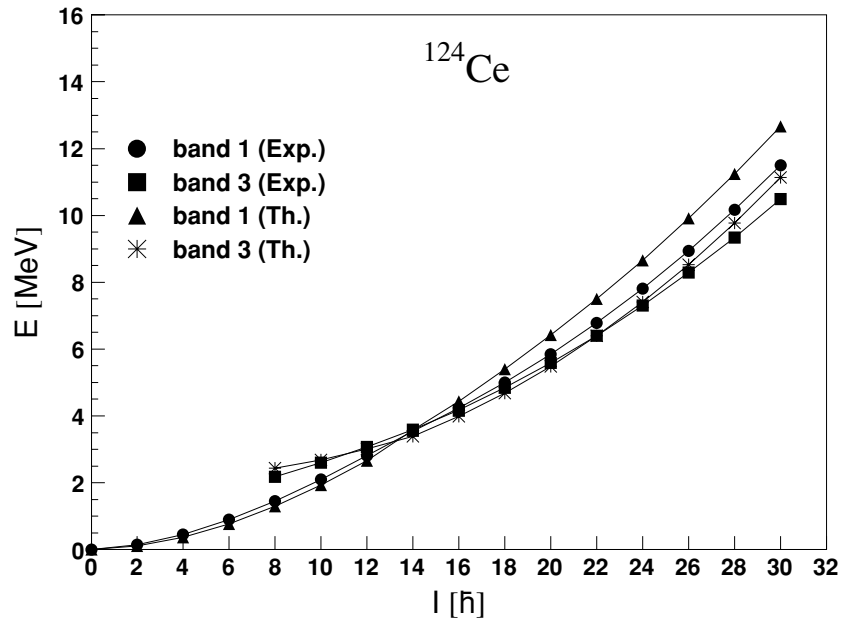

FIG. 7. Comparison of experimental and calculated excitation energies for positive parity bands (band 1 (Exp) and band 3 (Exp) correspond to experimental bands of Ref. [1]) in ^{124}Ce.

configurations to different bands in ^{124}Ce. For example, band 1 was assigned 0-qp configuration at low spin whereas band 3 was assigned $\pi h_{11/2}[541]3/2^- + \pi h_{11/2}[550]1/2^-$ configuration, giving $K = 2$. In the present PSM calculations, it turns out that the low lying states from $I = 0$ to $I = 12$ of band 1 belong to the pure 0-qp configuration in agreement with the results of Smith *et al*. However, for higher spin states of this band each state is found to be a superposition of states arising from different configurations with different weight factors. The various configurations that contribute to band 1 with weight factors $\geqslant$0.15 alone are listed in Table I. Besides 0-qp configurations, the other configurations that contribute are 2-qp $\nu h_{11/2}[5/2, 7/2]$, $K = 1$ and $\pi h_{11/2}[3/2, 5/2]$, $K = 1$. Above spin 22, the 4-qp $\nu h_{11/2}[5/2, 7/2] + \pi h_{11/2}[1/2, 1/2]$, $K = 1$ becomes dominant with weight factors $\geqslant$0.15.

In the case of band 3, the present calculation reveals that, it is based on $\pi h_{11/2}[3/2, 3/2]$ configuration, giving a possibility of $K = 0$. The weight factor for spin $I = 8$ is 0.65. As one goes to higher spins, it is observed that these states are a mixture of 2-qp configurations $\pi h_{11/2}[3/2, 3/2]$, $K = 0$ and $\pi h_{11/2}[1/2, 3/2]$, $K = 1$.The results are presented in Table I. It is noted from the table that both these configurations are dominant up to spin $I = 12$. Above spin $I = 14$, the states belonging to band 3 become a part of the yrast band up to highest spin observed. But the states after $I = 20$ are seen to arise from the superposition of two 4-qp bands with configurations $\nu h_{11/2}[5/2, 7/2] + \pi h_{11/2}[1/2, 3/2]$, $K = 2$ and $\nu h_{11/2}[5/2, 7/2] + \pi h_{11/2}[3/2, 3/2]$, $K = 1$. Besides this, in the work of Smith *et al*. the theoretical values of energies of various angular momentum states of band 1 and band 3 have not been presented. The aligned angular momentum versus spin plots predict backbending in band 1 at rotational frequency $\omega = 0.34$ MeV/$\hbar$. Our results predict the backbending at $\omega = 0.36$ MeV/$\hbar$. The CWS calculation also predicts second backbending at $\omega = 0.39$ MeV/$\hbar$ which is not observed experimentally. Our results on yrast band do not exhibit second backbending. Broadly speaking, the source of difference between the results of the present calculation and that of Smith *et al*. arises because of the following:

Firstly, Smith *et al*. carry out a CSM calculation based on Woods Saxon potential. In this model there is no mixing among different bands. It is because of this reason that each positive parity band is assigned one specific configuration. In

TABLE I. Predicted configurations and weight factors for energy states belonging to positive parity bands in ^{124}Ce.

	Band 1		Band 3	
$I[\hbar]$	Configurations	Weight factors	Configurations	Weight factors
2	0-qp	0.95		
4	0-qp	0.93		
6	0-qp	0.89		
8	0-qp	0.84	$\pi h_{11/2}$[3/2,3/2],K = 0	0.65
10	0-qp	0.75	$\pi h_{11/2}$[3/2,3/2],K = 0	0.39
			$\pi h_{11/2}$[1/2,3/2],K = 1	0.31
			$\pi h_{11/2}$[1/2,3/2],K = 2	0.15
12	0-qp	0.63	$\pi h_{11/2}$[3/2,3/2],K = 0	0.36
	$\nu h_{11/2}$[5/2,7/2],K = 1	0.16	$\pi h_{11/2}$[1/2,3/2],K = 1	0.22
14	0-qp	0.38	$\pi h_{11/2}$[1/2,3/2],K = 1	0.27
	$\nu h_{11/2}$[5/2,7/2],K = 1	0.23	$\pi h_{11/2}$[1/2,3/2],K = 2	0.15
	$\pi h_{11/2}$[3/2,3/2],K = 0	0.15		
16	0-qp	0.32	$\pi h_{11/2}$[1/2,3/2],K = 1	0.27
	$\nu h_{11/2}$[5/2,7/2],K = 1	0.28	$\pi h_{11/2}$[1/2,3/2],K = 2	0.15
			$\pi h_{11/2}$[3/2,3/2],K = 0	0.20
18	0-qp	0.25	$\pi h_{11/2}$[1/2,3/2],K = 1	0.22
	$\nu h_{11/2}$[5/2,7/2],K = 1	0.24	$\pi h_{11/2}$[3/2,3/2],K = 0	0.18
	$\pi h_{11/2}$[3/2,5/2],K = 1	0.17		
20	0-qp	0.16	$\pi h_{11/2}$[1/2,3/2],K = 1	0.18
	$\nu h_{11/2}$[5/2,7/2],K = 1	0.19	$\pi h_{11/2}$[3/2,3/2]K = 0	0.15
	$\pi h_{11/2}$[3/2,5/2],K = 1	0.17		
22	$\pi h_{11/2}$[3/2,5/2],K = 1	0.16	$\nu h_{11/2}[5/2, 7/2] + \pi h_{11/2}$[1/2,3/2],K = 2	0.17
			$\nu h_{11/2}[5/2, 7/2] + \pi h_{11/2}$[3/2,3/2],K = 1	0.16
24	$\nu h_{11/2}[5/2, 7/2] + \pi h_{11/2}$[1/2,1/2],K = 1	0.17	$\nu h_{11/2}[5/2, 7/2] + \pi h_{11/2}$[1/2,3/2],K = 2	0.22
			$\nu h_{11/2}[5/2, 7/2] + \pi h_{11/2}$[3/2,3/2],K = 1	0.22
26	$\nu h_{11/2}[5/2, 7/2] + \pi h_{11/2}$[1/2,1/2],K = 1	0.22	$\nu h_{11/2}[5/2, 7/2] + \pi h_{11/2}$[1/2,3/2],K = 2	0.25
	$\nu h_{11/2}[5/2, 7/2] + \pi h_{11/2}$[3/2,5/2],K = 0	0.15	$\nu h_{11/2}[5/2, 7/2] + \pi h_{11/2}$[3/2,3/2],K = 1	0.24
28	$\nu h_{11/2}[5/2, 7/2] + \pi h_{11/2}$[1/2,1/2],K = 1	0.24	$\nu h_{11/2}[5/2, 7/2] + \pi h_{11/2}$[1/2,3/2],K = 2	0.25
	$\nu h_{11/2}[5/2, 7/2] + \pi h_{11/2}$[3/2,5/2],K = 0	0.15	$\nu h_{11/2}[5/2, 7/2] + \pi h_{11/2}$[3/2,3/2],K = 1	0.26
30	$\nu h_{11/2}[5/2, 7/2] + \pi h_{11/2}$[1/2,1/2],K = 1	0.21	$\nu h_{11/2}[5/2, 7/2] + \pi h_{11/2}$[1/2,3/2],K = 2	0.24
	$\nu h_{11/2}[5/2, 7/2] + \pi h_{11/2}$[1/2,3,2],K = 2	0.16	$\nu h_{11/2}[5/2, 7/2] + \pi h_{11/2}$[3/2,3/2],K = 1	0.25

our model (PSM) mixing among 67 bands is done allowing one the freedom of assigning more than one configurations to the different or same state of a particular band. Secondly, it is well known that cranking calculation involves approximate angular momentum projection.

IV. CONCLUSIONS

Summarizing, the positive parity bands in ^{124}Ce has been studied by employing quadrupole-plus monopole and quadrupole pairing force within the framework of projected shell model approach. The transition quadrupole moments and g-factors show corresponding variations at the band crossing. The pronounced jump in g-factors at $I = 14$ is due to the proton 2-qp band crossing. The wave functions of yrast states at $I = 14$ to 20 are dominated by the proton 2-qp states, thus, enhancing the g-factor values. Thus, the measurement of Q_t and g-factors for ^{124}Ce would be a strong test for our predictions. The experimentally observed positive parity bands are reproduced very well in PSM calculations. From the predicted configurations, it seems that these bands do not belong to a single configuration but there is mixing of 2-qp and 4-qp configurations in high-spin states of ^{124}Ce. The work on the systematic study of other nuclei in $A = 120$–130 mass region is under progress.

ACKNOWLEDGMENTS

We are grateful to Dr. Y. Sun for providing guidance to pursue the present work. The first author (R.D.) acknowledges the Department of Science and Technology, New Delhi, for financial support.

[1] J. F. Smith, V. Medina-Chico, C. J. Chiara, M. P. Carpenter, C. N. Davids, M. Devlin, J. L. Durell, D. B. Fossan, S. J. Freeman, R. V. F. Janssens, D. R. LaFosse, M. J. Lebby, P. Reiter, D. G. Sarantites, D. Seweryniak, K. Starosta, R. Wadsworth, A. N. Wilson, and J. N. Wilson, Phys. Rev. C **69**, 034339 (2004).
[2] K. Hara and Y. Sun, Int. J. Mod. Phys. E **4**, 637 (1995).
[3] K. Hara and Y. Sun, Nucl. Phys. **A529**, 445 (1991).
[4] Y. Sun and J. L. Egido, Nucl. Phys. **A580**, 1 (1994).
[5] J.-Y. Zhang, N. Xu, D. B. Fossan, Y. Liang, R. Ma, and E. S. Paul, Phys. Rev. C **39**, 714 (1989).
[6] Y. Sun and M. Guidry, Phys. Rev. C **52**, R2844 (1995).
[7] S. Raman, C. H. Malarkey, C. W. Nestor, and P. Tikkanen, At. Data Nucl. Data Tables **78**, 1 (2001).